PoE-Enabled Visible Light Positioning Network With Low Bandwidth Requirement and High Precision Pulse Reconstruction

Zhenghai Wang, *Member, IEEE*, Xuan Huang, *Graduate Student Member, IEEE*, Xuanbang Chen, *Graduate Student Member, IEEE*, Mengzhen Xu, *Student Member, IEEE*, Xiaodong Liu, *Member, IEEE*, Yuhao Wang, *Senior Member, IEEE*, and Xun Zhang, *Senior Member, IEEE*

***Abstract*—The power over Ethernet (PoE)-enabled visible light positioning (VLP) networks as a promising technology can significantly enhance accuracy and cost-effectiveness of indoor positioning. However, both the limited bandwidth of the light-emitting diode (LED) and the low sampling rate of the receiver have a negative impact on the positioning performance. Moreover, time synchronization requirements between transmitters and between transceivers become more stringent in a resource-constrained VLP network. To address these issues, a PoE-enabled VLP scheme with low bandwidth requirement and high-precision pulse reconstruction is proposed in this article. Specifically, the precision time protocol and synchronous Ethernet are introduced to realize the synchronization transmission. Meanwhile, an ON–OFF keying (OOK) modulation-based beacon signal is designed to unlock both the transceivers' synchronization and bandwidth requirements. Then, a high-precision pulse reconstruction method considering the LED model and impulse response is established to enhance the signal quality. Moreover, the position is estimated based on the maximum a posteriori (MAP) probability criterion. Experimental results obtained by the VLP testbed demonstrate that the proposed scheme outperforms the benchmark positioning schemes. It achieves a positioning accuracy of 1.7 cm by using the reconstructed 2 GHz sampling rate in the case of a bandwidth of 50 MHz and a real sampling rate of 100 MHz. Last but not least, the proposed scheme maintains positioning accuracy within 30 cm even with a few MHz bandwidth of LED.**

***Index Terms*—Beacon design, power over Ethernet (PoE), sampling rate, synchronization, visible light positioning (VLP).**

I. Introduction

FULL spectrum communication and positioning, including sub-6 GHz, mmWave, THz, and visible light band-enabled technology, is emerging as a valuable solution to tackle the challenges of spectrum resource scarcity and the higher key performance indicators required for 6G networks, especially integrated sensing and communication requirement [1], [2]. Thanks for the prominent energy saving and long life advantages of light-emitting diode (LED), LED-based illumination has become the mainstream infrastructure [3], [4]. Thus, it is natural that visible light band-based wireless communication and sensing systems have emerged as promising enabling technologies in the era of 6G. Specifically, based on the densely distributed LEDs and corresponding rich and license-free spectrum resources, the development of indoor visible light positioning (VLP) technologies can solve the problems of both the poor indoor propagation quality and inadequate positioning accuracy associated with existing wireless positioning systems, which is very suitable for enhancing the indoor positioning performance [5], [6].

Naturally, how to effectively collaborate with distributed multiple LEDs to utilize the full potential of LED resources is a crucial issue that cannot be ignored [7]. IEEE 802.3bt standard-based power over Ethernet (PoE) technology can transmit both energy and information simultaneously over the same cable, offering an opportunity to support LED-based illumination and wireless information services. Thus, the PoE-based wire link can effectively distribute the required energy and data to VLP access points (APs) [8]. Specifically, the PoE can enhance the energy efficiency of the entire LED-based VLP network with

Manuscript received 8 November 2023; revised 28 November 2023; accepted 4 December 2023. Date of publication 13 December 2023; date of current version 29 December 2023. This work was supported in part by the National Natural Science Foundation of China under Grant 62161023 and Grant 62061030, in part by the Young Natural Science Foundation of Jiangxi Province under Grant 20224BAB212004, in part by the Graduate Innovation Special Foundation of Jiangxi Province under Grant YC2023-S140, in part by the EU Horizon 2020 program towards the 6G BRAINS project H2020-ICT 101017226. This paper was presented in part at IEEE IPIN 2023 [DOI: 10.1109/IPIN57070.2023.10332488]. *(Corresponding authors: Xiaodong Liu; Yuhao Wang.)*

Zhenghai Wang, Xuan Huang, Xuanbang Chen, and Mengzhen Xu are with the School of Information Engineering, Nanchang University, Nanchang 330031, China (e-mail: zhenghai.wang@ncu.edu.cn; huangxuan@email.ncu.edu.cn; chenxuanbang@email.ncu.edu.cn; xdream.zz@qq.com).

Xiaodong Liu is with the School of Information Engineering, Nanchang University, Nanchang 330031, China, and also with the Institut supérieur d'électronique de Paris (ISEP), 75006 Paris, France (e-mail: xiaodongliu@whu.edu.cn).

Yuhao Wang is with the School of Information Engineering, Nanchang University, Nanchang 330031, China, and also with the Digital Technology Application Industry College of Shangrao Normal University, Shangrao 334001, China (e-mail: wangyuhao@ncu.edu.cn).

Xun Zhang is with the Department of Electronic and Computer Engineering, Institut supérieur d'électronique de Paris (ISEP), 75006 Paris, France (e-mail: xun.zhang@isep.fr).

Digital Object Identifier 10.1109/JISPIN.2023.3342732

the help of the dc transmission format. Meanwhile, the PoE can also effectively provide large amounts of data to each AP based on the advantage of several hundred Mbps data transmission rates. Thus, the PoE-enabled VLP network is a forward-looking enabling sensing solution in practical indoor positioning vision. Numerous studies have been devoted to enhancing the positioning performance of VLP systems based on received signal strength (RSS), angle of arrival (AoA), time difference of arrival (TDOA) [9], [10], [11], [12], [13]. Specifically, Li et al. [9] proposed a fusion positioning scheme to estimate the accurate position of pedestrians in which a particle filter was used to process the fused data obtained from the hybrid VLP and inertial positioning system. For the multiple AP-enabled VLP system, a packet coding technique was introduced into time-division multiplexing in order to reduce positioning delay and enhance positioning performance [10]. Moreover, in [11], a two-phase hybrid RSS/AoA algorithm based on signal strength, azimuth, and elevation angle observation was proposed to achieve high-precision positioning. The authors in [12] proposed a novel spatial illumination patterns, which provide fingerprint optical signals for each spatial location and then the position information can be extracted from a time sequence of the proposed patterns. Furthermore, the authors in [13] considered the impact of noise sources such as shot noise, thermal noise, and wall-reflected light, and then estimated the receiver position based on the TDOA of visible light radiated by the LED panel. It is worth noting that these efforts can effectively enhance the accuracy of positioning in scenarios with abundant hardware resources. However, there are many resource-limited scenarios, especially in the Internet-of-Things (IoT) networks, the VLP system in these scenarios should meet the requirements of low hardware cost and power consumption. The authors in [14] and [15] pointed out that the direct utilization of low-cost photodiode (PD)-based receivers with low sampling rates may restrict the response to varying signals and decrease communication rates. Specifically, a low sampling rate is difficult to meet the Nyquist sampling rate, which results in undersampling and difficulty in accurately recovering the original signal. Moreover, due to the large junction capacitance and package inductance of LED, the bandwidth of LED is generally less than 10 MHz [16], [17]. The limited modulation bandwidth not only restricts the achievable signal modulation performance, but also impacts the integrity of the beacon signal. Thus, it is meaningful to investigate a suitable positioning scheme to alleviate both the bandwidth and sampling rate requirements in the resource-limited VLP systems. In the PoE-enabled VLP networks, besides the issues of both low modulation bandwidth and sampling rate under the resource-limitation case, strict synchronization is an urgent issue that needs to be solved. Specifically, to ensure the performance of the PoE-enabled VLP network, two types of synchronization must be efficiently fulfilled: synchronization between transmitters and synchronization between transceivers.

To address these issues, an indoor high-precision positioning scheme for the PoE-enabled VLP network is proposed. Based on the previous work [1], the PoE structure is exploited to transmit the energy and both positioning and dimming control information for each LED. In particular, the information transmission capability of PoE naturally offers a solution for intertransmission synchronization. Correspondingly, the time and frequency synchronization of the reference clock among the LED transmitters are realized with the aid of the synchronous Ethernet (SyncE) and precision time protocol (PTP). Meanwhile, a novel beacon is designed to unlock the time synchronization between the transceivers. Thus, the positioning scheme does not require stringent time synchronization. Moreover, the proposed scheme achieves high positioning performance with a low sampling rate and low bandwidth. The main contributions are summarized as follows.

1) Inspired by the ease of implementing both information and illumination services with limited modulation bandwidth, the PoE-based ON–OFF keying (OOK) modulation is exploited in the considered VLP networks to tackle the synchronization and illumination requirement among LED. First, both the time and frequency synchronization among the LED are realized through the SyncE and PTP. Meanwhile, the dimming and beacon control are sent to each LED through the PoE structure. Then, the OOK-based pulse pairs are generated in each LED to construct the positioning beacon signal and to tackle the synchronization requirement of the transceiver.
2) Considering the challenge of signal distortion caused by both the low sampling rate and the LED circuit distortion under the case of limited hardware resources, an LED equivalent model is introduced to facilitate signal reconstruction and the corresponding high-precision pulse reconstruction method is established to eliminate the distortion effect and reduce the time interval between sampling points. Subsequently, a positioning method based on the maximum a posteriori (MAP) probability criterion is proposed to estimate the location from the reconstructed signal.
3) A semiphysical experimental testbed is established to validate the performance of the proposed positioning scheme. Specifically, the beacon signal is transmitted by the PoE-enabled LED front-end. Then, based on the MAP, the location is estimated from the data, which is measured from the receiver with a low sampling rate of 100 MHz. The experimental results show that the proposed scheme with a reconstructed 2 GHz sampling rate achieves a positioning accuracy of 1.7 cm. Moreover, compared with existing positioning benchmark schemes, which are based on the differential phase difference of arrival (DPDOA), TDOA, RSS, and camera-assisted RSS (CA-RSS), the results reveal the superior positioning performance of the proposed scheme.

The rest of this article is organized as follows. Section II introduces the system model, the synchronization transmission, and the design details of positioning beacon. In Section III, the high-precision pulse reconstruction method and the positioning processing based on the MAP are described. Then, the semiphysical experimental testbed and experimental analysis are carried out in Section IV. Finally, Section V concludes this article.

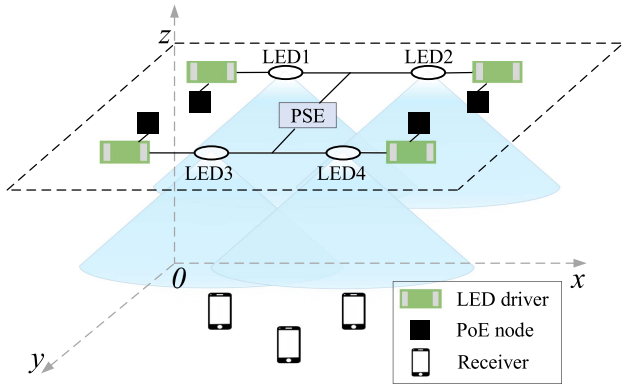

Fig. 1. PoE-enabled VLP network structure.

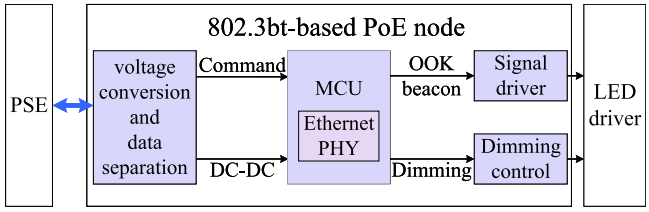

Fig. 2. Scheme diagram of the PoE-enabled LED transmitter end.

II. System Model and Synchronization Scheme

A. System Model

In a typical indoor scenario, three LEDs are generally the minimum positioning requirement to achieve accurate positioning. Moreover, even number of lamps are usually installed to achieve uniform illumination. Thus, as shown in Fig. 1, four LEDs are uniformly deployed in the ceiling. In order to facilitate deployment with lower costs and enhance the energy efficiency of the VLP networks, the PoE wire cable is employed to transfer power and data. Note that the data include the dimming and beacon data control information. Correspondingly, the PoE node extracts the energy, positioning, and dimming command from the data stream in the cable. Then, the OOK-based beacon is transmitted by the LED and positioning information is extracted and estimated from the received signal.

Based on the considering VLP configuration, the scheme diagram of the PoE-enabled LED transmitter end is shown in Fig. 2. Specifically, the power sourcing equipment (PSE) module transmits the dc power and the IP package through the PoE cable. Then, the rectifier and data separation module is exploited to extract the dimming and positioning information from the IP data. Meanwhile, it is also used to convert the dc competent to enhance the energy efficiency of power transmission. Moreover, the microcontroller unit (MCU) in the PoE node generates the OOK modulation beacon based on the extracted OOK modulation command. Furthermore, the dimming control module is exploited to generate the dimming signal by the corresponding command. In addition, the beacon signal, which processed by the signal driver module and the dimming signal are superimposed and then input to the LED driver to generate the final OOK positioning signal for transmission.

The proposed positioning scheme first performs OOK modulation in the ith LED and forms a positioning beacon signal $x_i[t]$. Then, the received signal from kth pulse pair of the ith LED to location $\boldsymbol{q}_j$ is defined as

$$y_{i,j}(k) = \sqrt{P_i} \times h_{i,j} \times x_i[\phi_i(k) + \tau_{i,j}] + n_0 \tag{1}$$

where P_i is the radiation optical power of the ith LED, $h_{i,j}$ is the channel gain between the ith LED and the jth PD. Moreover, $\phi_i(k)$ is the radiation time of the kth pulse pair at the ith LED, $\tau_{i,j}$ is the transmission time of the coded pulse pair between the ith LED, and the jth PD. Channel noise n_0 obeys the Gaussian distribution.

Since the channel gain is inversely proportional to the square of the distance, the non-line-of-sight (NLoS) gain is much weaker than the line-of-sight (LoS) gain. Without loss of generality, it is safe to assume that the LoS path dominates the channel gain [18]. Moreover, it is assumed that the LED radiation model follows the Lambertian model. Therefore, the channel gain $h_{i,j}$ is expressed as [18]

$$h_{i,j} = \frac{(m_0+1)A_{\mathrm{PD}}}{2\pi d_{i,j}^2} \cos^{m_0}(\phi) \cos(\varphi) G(\varphi) T(\varphi) \tag{2}$$

where $d_{i,j}$ is the distance between the ith LED (x_i, y_i, z_i) and the jth PD (x_j, y_j, z_j). m_0 is the Lambertian order of the LED. A_{PD} is the detection area of PD. $G(\varphi)$ and $T(\varphi)$ are the gains of optical filters (OF) and optical concentrators (OC), respectively. Moreover, ϕ and φ are the radiation angle and incident angle between the LED and PD. It is assumed that the normals of the LED and PD are parallel to each other. Thus, given the channel gain $h_{i,0}$ and distance $d_{i,0}$ from the ith LED to the reference position (x_0, y_0, z_0), the relationship between the path channel gain $h_{i,j}$ and distance $d_{i,j}$ from the ith LED signal to jth PD is expressed as

$$h_{i,j} = h_{i,0} \left(\frac{d_{i,0}}{d_{i,j}} \right)^{m_0+3}. \tag{3}$$

Based on (1), the signal $y_{i,j}(k)$ received from the emission pulse at time $\phi_i(k)$ follows the Gaussian distribution, and it is given by

$$p(y_{i,j}(k)|\phi_i(k)) = \mathcal{N}\left(h_{i,j} \sqrt{P_i w_{j,\phi_i}(k) T_{\mathrm{w}}}, \sigma^2 \right) \tag{4}$$

where the Gaussian distribution with mean μ and variance σ^2 is denoted by $\mathcal{N}(\mu, \sigma^2)$. For the mean item in (4), $w_{j,\phi_i}(k)$ quantifies the ratio of the overlap time $\Delta t_{i,j}(k)$ between the expected pulse observation window and the actual observation window to the pulsewidth T_{w}, and it is calculated as

$$w_{j,\phi_i}(k) = \begin{cases} \frac{\Delta t_{i,j}(k)}{T_{\mathrm{w}}}, & \Delta t_{i,j}(k) > 0 \\ 0, & \Delta t_{i,j}(k) \le 0 \end{cases} \tag{5a}$$

$$\Delta t_{i,j}(k) = T_{\mathrm{w}} - \left| \phi_i(k) + \frac{d_{i,j}}{c} - t_{i,j}(k) \right| \tag{5b}$$

where c is the light speed, $t_{i,j}(k)$ is the arrival time of the kth pulse pair, and $|a|$ represents the absolute value of a. However, because of differences in transmission distances between the

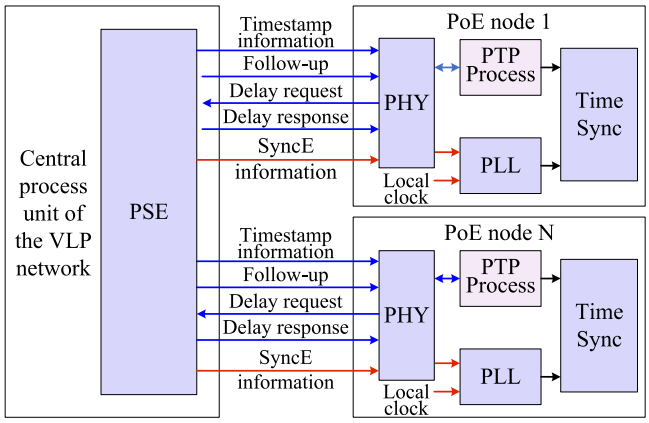

Fig. 3. Construction of synchronization transmission.

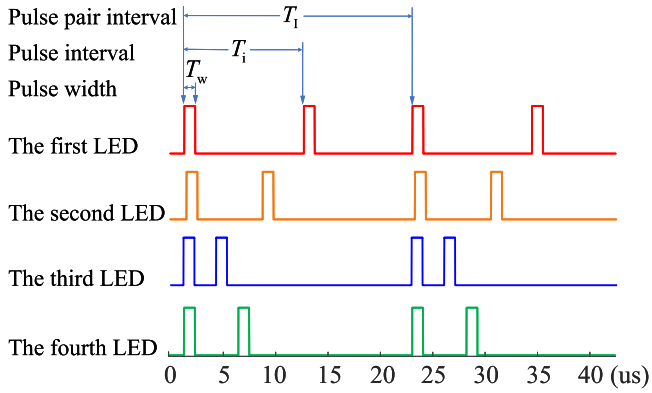

Fig. 4. Example of positioning beacon design with the four LEDs.

PSE and each LED-based transmitter AP, it is necessary to address the issue of reference clock frequency and time synchronization among the LED-based transmitter APs.

B. Synchronization Transmission

In order to tackle the synchronization transmission, the SyncE and the PTP are exploited to realize the reference clock frequency synchronization and the clock synchronization requirement among the LED-based transmitter APs, respectively [19]. Fig. 3 illustrates the synchronization transmission details based on the SyncE and PTP. Specifically, timestamp messages, follow-up messages, and delay responses are sequentially sent through IP packets according to the PTP. In response, the port physical layer (PHY) in the PoE node receives these messages and subsequently sends the delay request. This mechanism allows the PTP process module to achieve time and phase synchronization [20], [21]. Moreover, a high-precision clock information is inserted into the IP packet, and the corresponding SyncE information is extracted by the PHY of PoE node. It then controls the phase-locked loop to generate the desired reference frequency clock [22]. Furthermore, the time synchronization between the transmitters are achieved based on the time, phase, and frequency signal. It is worth noting that the proposed method integrating the PTP and SyncE can achieve time synchronization and working frequency synchronization among different PoE nodes and thus the time synchronization accuracy between the transceivers is controlled within 1 ns instead of microsecond level [19]. Finally, the impact of positioning error caused by this synchronization time error is considered and solved in Section III.

C. Positioning Beacon Design

Considering the fact that the modulation bandwidth of LED is limited in the low cost and resource-constrained VLP system. The bandwidth-friendly OOK modulation is chosen to construct the positioning beacon. However, the low switching rate and response time lead to a slow rise speed of the OOK modulation pulse. In other words, the traditional OOK modulation-based positioning scheme is difficult to obtain high-precision performance [23]. Therefore, a novel OOK-based coded pulse pair is proposed to inherit the bandwidth-cost advantage of OOK and alleviate the limitation of OOK. The main idea behind this beacon is to design pulse sequences with a different time intervals for each LED.

The example of the positioning beacon design profile with four LEDs is shown in Fig. 4. It can be seen that each LED has an equal pulsewidth T_{w} and a pulse pair interval T_{I} ($T_{\mathrm{I}} = NT_{\mathrm{w}}$, N is any positive integer). In order to ensure that the PD can distinguish at least four complete pulse pairs and extract information from each LED pulse pair, the guidelines of this positioning beacon and the practical choice of the interval parameters are given as follows. First, in order to facilitate the receiver to distinguish the beacons of different LEDs, the pulse interval T_i of each LED is required to be different from that of other LEDs, and any two pulse intervals T_i and T_j are mutually prime. Moreover, the pulse interval T_i is much larger than $(\tau_{\mathrm{t,max}} + \tau_{\mathrm{e,max}})$ to avoid overlap between pulses, where $\tau_{\mathrm{t,max}}$ and $\tau_{\mathrm{e,max}}$ denote the maximum transmission delay in the considered indoor space and the upper limit of time error, respectively. Furthermore, the pulse pair interval T_{I} is greater than any pulse interval T_i to ensure that all beacon signals can be transmitted in a pulse pair interval T_{I}. Note that the pulse position modulation can be also employed to achieve the beacon, it holds promise for achieving better performance in systems with more abundant resources.

III. Pulse Reconstruction and Position Estimation

The positioning beacon signal through the channel is obtained by the PD of receiver. Then, the receiver processes the received signal to extract the corresponding beacon each LED. Due to the strong dependence of the positioning performance on the sampling rate and signal integrity, it is important to provide a high sampling rate and high quality signal for achieving high-accuracy positioning. However, a high sampling rate in the receiver significantly increases the cost and power consumption of the receiver, while the hardware resources and energy in the receiver are usually limited. Moreover, signal integrity is influenced by the limited modulation bandwidth of the LED. Furthermore, the signal distortion and jitter resulting from the LED also affect the quality of the positioning beacon signal and consequently decrease the positioning performance.

In order to achieve enough positioning performance in a low cost and low power consumption in resource-limited VLP network, a high-precision pulse reconstruction method is proposed. Specifically, a high sampling rate pulse is initially obtained from the resource-limited low sampling rate pulse sequence by using the sampling rate conversion method. Then, the signal is recovered by considering the LED-based pulse response and the minimum mean-square error (MSE) principle. Finally, a MAP-based position estimation method is proposed. The details of the proposed high-precision pulse reconstruction and corresponding position estimation method are given as follows.

A. High-Precision Pulse Reconstruction

This section introduces a precision pulse reconstruction method based on the rational factor sampling rate conversion, which can reconstruct discrete-time signals under ideal conditions and resample continuous-time signals at different sampling rates. For any continuous-time signal $x(t)$, a discrete-time signal $x(n)$ can be obtained by the sampling rate of $f_x = 1/T_x$. Then, based on the sampling theorem, $x(n)$ can be converted to a continuous-time signal $y(t)$, and $y(t)$ is defined as

$$y(t) = \sum_{n=-\infty}^{\infty} x(nT_x)g(t - nT_x) \tag{6}$$

where $g(t - nT_x)$ is the reconstruction function. According to the sampling theorem, the recovery of $y(t)$ from $x(n)$ requires an infinite number of samples. However, due to the finite number of samples of the signal and the practical constraints associated with finite duration signals, the reconstruction of the original $x(t)$ from $y(t)$ is difficult in a practical scenario. In practice, the reconstruction signal $y(mT_y)$ with a high sampling rate of $f_y = 1/T_y$ is given as

$$y(mT_y) = \sum_{n=-\infty}^{\infty} x(nT_x)g\left(mT_y - nT_x\right) \tag{7}$$

where nT_x and mT_y correspond to the input and output time of the signal, respectively. Equation (7) represents a linear time-invariant system in the case of the sampling rate $f_x = f_y$. On the contrary, when $f_x \neq f_y$, it is reformulated by changing the sum index variable from n to $k = k_m - n$ and is given by

$$y\left(mT_y\right) = \sum_{k=-\infty}^{\infty} x\left(\left(k_m - k\right)T_x\right)g\left(kT_x + \Delta_m T_x\right) \tag{8}$$

where $k_m = \lfloor mT_y/T_x \rfloor$ and $\Delta_m = mT_y/T_x - k_m$, the $\lfloor\cdot\rfloor$ denotes floor function. The key in the reconstruction process is to determine the corresponding value of $g(t - nT_x)$. Thus, in order to facilitate this reconstruction process, the ratio of $T_y/T_x = D/I$ is limited as a rational number. Then, Δ_m has only I unique values. The corresponding $g_m(nT_x)$ has I different value sets, and it has a period of m, namely,

$$g_m\left(nT_x\right) = g_{m+rI}\left(nT_x\right), \quad r = 0, \pm1, \pm2, \ldots. \tag{9}$$

Then, the process of upsampling and downsampling is introduced. For the upsampler, the $g_m(nT_x)$ is processed by an integer factor I to increase the sampling rate. Specifically, by replacing T_y with IT_x, $y(mT_y)$ can be redefined as

$$y(mT_y) = \sum_{k=-\infty}^{\infty} x(kT_x)g(m(T_x/I) - kT_x). \tag{10}$$

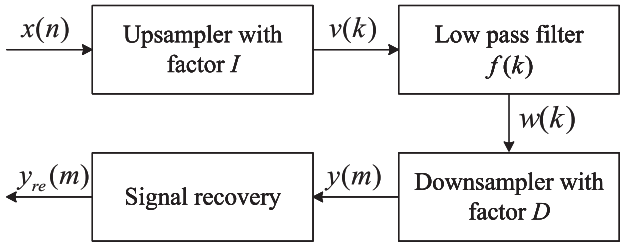

Fig. 5. Proposed high-precision pulse reconstruction structure.

For the downsampler, it involves reducing the sampling rate using an integer factor D. Specifically, by replacing T_y with DT_x, $y(mT_y)$ can be redefined as

$$y(mT_y) = \sum_{k=-\infty}^{\infty} x(kT_x)g((mD - k)T_x). \tag{11}$$

It is worth noting that both $x(t)$ and $g(t)$ are sampled at a period of T_x. In order to preserve the spectral characteristics of the original signal as much as possible, the proposed high-precision pulse reconstruction is conducted by first interpolating and then sampling. Based on the above principles, the details of the proposed high-precision pulse reconstruction structure are shown in Fig. 5.

Specifically, based on the upsampler with factor I, $I - 1$ zeros are first inserted between adjacent sample points of $x(n)$ to achieve the upsample signal $v(k)$. The output sequence of the upsampler in the time domain is expressed as

$$v(k) = \begin{cases} x(k/I), & k = 0, \pm I, \pm 2I, \ldots \\ 0, & \text{otherwise.} \end{cases} \tag{12}$$

Then, the filter is utilized to remove the unnecessary frequency components in $v(k)$. Note that the frequency response $F(\omega_v)$ of the low-pass filter must balance the effects of upsampling and downsampling. Thus, $F(\omega_v)$ is given by

$$F\left(\omega_v\right) = \begin{cases} I, & 0 \leq |\omega_v| \leq \min(\pi/D, \pi/I) \\ 0, & \text{otherwise.} \end{cases} \tag{13}$$

Thus, the output sequence $w(k)$ of low-pass filter is expressed as

$$w(k) = \sum_{k=-\infty}^{\infty} f(k - kI)x(k). \tag{14}$$

Moreover, the signal $y(mT_y)$ is extracted from $w(k)$ using the downsampler with factor D. Since the T_y exists only to distinguish the sampling rate of the input signal, the output sequence $y(mT_y)$ is simplified to $y(m)$ and it is defined as

$$y(m) = \sum_{k=-\infty}^{\infty} f(mD - kI)x(k) \tag{15}$$

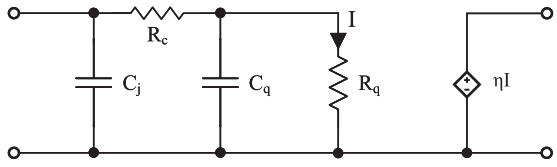

Fig. 6. Voltage drive LED model.

where $k = \lfloor mD/I \rfloor - n$. Thus, for the input signal $x(n)$ with sampling rate f_x, the sampling rate of the reconstructed signal $y(m)$ is $(If_x)/D$. The spectrum of the output sequence $y(m)$ can be obtained and it is written as

$$Y(\omega_y) = \begin{cases} \frac{I}{D} X\left(\frac{\omega_y}{D}\right), & 0 \le |\omega_y| \le \min\left(\pi, \frac{\pi D}{I}\right) \\ 0, & \text{otherwise} \end{cases} \tag{16}$$

where $X(w)$ is the spectrum response of the input signal $x(n)$.

The output sequence $y(m)$ obtained by the above process is a high-resolution digital signal. However, the received VLP signal is still distorted due to the limited bandwidth of the LED. Specifically, the LED limited bandwidth slows down the edges of the signal. Thus, a signal recovery module based on both the voltage drive LED model and corresponding impulse response is introduced to improve the accuracy of reconstructed signals. The voltage drive LED model is widely recognized as Fig. 6 and the corresponding physics-based LED frequency response $H(\omega)$ can be written as [24]

$$H(\omega) = \frac{\eta}{1 - \omega^2 R_c R_q C_q C_j + \omega(R_q C_q + R_c C_j + R_q C_j)} \tag{17}$$

where η represents the external quantum efficiency. R_{c} and R_{q} are the equivalent resistances of the cladding layer and quantum well, respectively. C_{q} is the capacitance of the quantum well and C_{j} is the sum of the barrier capacitance and the parasitic capacitance. Note that the parameters in the model can be extracted by measuring the impedance or frequency response of the LED. The impulse response vector of LED can be written as

$$\boldsymbol{h_l} = \begin{bmatrix} h_l(0) & h_l(1) & h_l(2) & \dots & h_l(M-1) \end{bmatrix} \tag{18}$$

where the discrete response is calculated by

$$h_l(m) = \frac{1}{M} \sum_{K=0}^{M-1} H\left(\frac{Kf_y}{M}\right) e^{i\frac{2\pi}{M}mK}, \quad m = 0, 1, \dots, M-1 \tag{19}$$

where M is the length of $y(m)$. The main idea behind the signal recovery is find an estimated matrix $\boldsymbol{W}$ based on the MSE principle to recover the received signal to reconstruction signal vector $\hat{\boldsymbol{s}}$. First, the vector error $\boldsymbol{e}$ between the reconstruction and transmission signal vector is defined as

$$\boldsymbol{e} = \hat{\boldsymbol{s}} - \boldsymbol{s} = \mathbf{W}^* \boldsymbol{y} - \mathbf{s} \tag{20}$$

where $\boldsymbol{y}$ represent the vector of the high-precision reconstructed signal sequence $[y(1)\ y(2)\ \dots\ y(m)]$ and the $(\cdot)^*$ denotes the conjugate transpose. Then, the MSE is written as

$$\boldsymbol{e}_{\mathrm{MSE}} = \mathbb{E}\left(||\mathbf{W}^* \boldsymbol{y} - \mathbf{s}||^2\right) \tag{21}$$

where $\mathbb{E}(\cdot)$ denotes the mathematical expectation and $||\cdot||$ represents the second-order norm. In the case of that the error converges to the minimum and the correlation between $\boldsymbol{y}$ and $\boldsymbol{e}_{\mathrm{MSE}}$ is zero, the optimal matrix $\boldsymbol{W}_{\mathrm{MMSE}}$ is calculated

$$\begin{aligned} \boldsymbol{W}_{\mathrm{MMSE}} &= \arg\min_{\boldsymbol{W}} \mathbb{E}||\mathbf{W}^* \boldsymbol{y} - \mathbf{s}||^2 \\ &= \mathbf{R_s} \boldsymbol{h}^* (\boldsymbol{h} \mathbf{R_s} \boldsymbol{h}^* + \boldsymbol{R_n})^{-1} \end{aligned} \tag{22}$$

where $\boldsymbol{R_s}$ denotes the autocorrelation matrix of transmission signal $\boldsymbol{s}$ and $\boldsymbol{R_n}$ is the autocorrelation matrix of the Gaussian distribution noise in the context.

B. MAP-Based Position Estimation

MAP is a probability estimation method based on the Bayesian theorem, which is used to estimate the most likely value of an unknown random variable under the condition of given observations. The goal of MAP estimation is to find the parameter value with the maximum posterior probability, where the posterior probability refers to the conditional probability of the parameter value in the case of a given observation [25]. Based on the MAP detector, the optimal location $\hat{\boldsymbol{q}}_{j\,\mathrm{MAP}}$ for the jth PD estimated by the proposed scheme is given by

$$\begin{aligned} \hat{\boldsymbol{q}}_{j\,\mathrm{MAP}} &= \arg\max_{r_j} p\left(r_j | y_{\mathrm{re}}\right) \\ &\overset{(a)}{=} \arg\max_{r_j} p\left(r_j | y_{\mathrm{re},1}, y_{\mathrm{re},2}, y_{\mathrm{re},3}, y_{\mathrm{re},4}\right) \\ &= \arg\max_{r_j} \prod_{i=1}^{4} \left[\int_{\boldsymbol{\Phi}_i} \frac{p\left(y_{\mathrm{re},i} | \phi_i\right) p(\phi_i, j)}{p\left(y_{\mathrm{re},i}\right)} d\phi_i \right] \end{aligned} \tag{23}$$

where $r_j = (x_j, y_j, z_j)$ denote the location of the jth PD. For the sake of notational simplicity, the reconstructed high sampling rate signal $y_{re}(m)$ is uniformly expressed as y_{re}. Then, $y_{\mathrm{re},i}$ is the reconstructed signal corresponding to the ith LED. The process (a) holds since y_{re} is composed of $y_{\mathrm{re},i}$. Moreover, $\boldsymbol{\Phi}_i$ is the set of all possible radiation times ϕ_i of the visible light pulse emitted by the ith LED. Since the measured time error and the terminal position distribution are independent and the random variables of both the measured time error and terminal position obey the uniform distribution, the joint probability $p(\phi_i, j)$ in (23) is rewritten as

$$p\left(\phi_i, j\right) = p\left(\phi_i\right) p(j) = \frac{1}{|\boldsymbol{\Phi}_i|} \times \frac{1}{|\mathbf{J}|} \tag{24}$$

where $\boldsymbol{\Phi}_i$ and $\mathbf{J}$ are the potentials of the measurement time value set and the terminal position value set, respectively.

In the time domain, the positioning method described in (23) mainly includes three types of time errors. First, the time error among the emission times of the pulse pair at each LED is caused by the difference in the arrival time of the pulse source to the LED. Note that this type of time error can be controlled within 1 ns with the introduction of PTP and SyncE-based synchronization transmission as presented by Section II [19]. Meantime, this time error remains unchanged once the cable layout is determined. The second type of time error results from the difference in the response of each LED. Fortunately, in order

to provide stable lighting, the performance difference between LEDs in the same network is small. As a result, its time error can be ignored. Finally, there is a random error in the arrival time of the pulse estimated by the terminal, it is caused by the link noise.

The first two errors determine the center value offset of the radiation time set $\mathbf{\Phi}_i$ in each LED. The third error determines the divergence degree of radiation time $\mathbf{\Phi}_i$. Moreover, since the pulse pairs from each LED to the same receiver are affected by the same link noise environment, it is reasonable to assume that the radiation time set $\mathbf{\Phi}_i$ of the four LEDs estimated by the receiver has the same characteristic in the proposed scheme. Thus, the joint probability of time error of each LED and jth PD in (24) are the same. Then, substituting (24) into (23), it can be further simplified as

$$\hat{\boldsymbol{q}}_{j\,\mathrm{MAP}} = \arg\max_{r_j} \prod_{i=1}^{4} \left[\int_{\mathbf{\Phi}_i} p\left(y_{\mathrm{re},i}|\phi_i\right) d\phi_i \right]. \tag{25}$$

In order to reduce the computational complexity, the logarithmic operation is applied to (25), and the mean value is calculated. Then, based on (3)–(5), the final positioning optimization problem is reformulated as

$$\mathrm{P}_0 : \min_{r_j} \sum_{k=1}^{K} \sum_{i=1}^{4} \left| y_{\mathrm{re},i}(k) - h_{i,j} \sqrt{P_i w_{\phi_i,j}(k) T_w} \right| \tag{26a}$$

$$\text{s.t.} \quad \mathrm{C1} : c\left|t_{i,0}(k) - \phi_i(k)\right| - d_{i,0} < \varepsilon \tag{26b}$$

$$\mathrm{C2} : (3)\text{–}(5) \tag{26c}$$

where tiny constant ε is the tolerable positioning error threshold. Moreover, $t_{i,0}(k)$ is the arrival time of the kth pulse pair observed by the receiver at the reference position. Then, the solving process for problem P_0 is introduced in the following.

Given the position error threshold ε, pulsewidth T_{w}, pulse interval T_{I}, LED coordinate (x_i, y_i, z_i), LED radiation power P_i, reference position coordinate (x_0, y_0, z_0), and time domain search progress factor α is given in the considering PoE-enable VLP network. The distance $d_{i,0}$ can be obtained. Meantime, for the fixed terminal at the reference position, the pulse signal is detected and the corresponding number of pulse pairs K is counted. $K \geq 1$ is enough to ensure the acquisition of valid location information. Then, the distinguishable pulse $y_{i,0}(k)$ and pulse arrival time $t_{i,0}(k)$ of the ith LED in the kth pulse pair interval are measured. Thus, the reconstructed signal $y_{\mathrm{re},i,0}(k)$ is obtained by using the proposed pulse reconstruction. Moreover, the channel gain $h_{i,0}$ and the radiation time $\phi_i(0)$ of 0th pulse pair are calculated as

$$h_{i,0} = \frac{1}{K \times \sqrt{P_i}} \sum_{k=0}^{K-1} y_{\mathrm{re},i,0}(k) \tag{27a}$$

$$\phi_i(0) = \frac{1}{K} \sum_{k=0}^{K-1} \left(t_{i,0}(k) - \frac{d_{i,0}}{c} - kT_{\mathrm{I}}\right). \tag{27b}$$

TABLE I
SIMULATION PARAMETERS

Parameter	Values	Parameter	Values
m_0	1	$l \times w \times h$	$5 \times 5 \times 3$ m^3
α	0.5	LED 1	(1.25,1.25,3)
ε	0.01 m	LED 2	(3.75,1.25,3)
T_{w}	1 μs	LED 3	(1.25,3.75,3)
T_{I}	21 μs	LED 4	(3.75,3.75,3)
P_i	0.3 W	(x_0, y_0, z_0)	(2.5,2.5,0)

Second, the time error is calculated as

$$\delta^2 = \frac{1}{K} \sum_{k=0}^{K-1} \left[t_{i,0}(k) - (d_{i,0}/c + \phi_i(k))\right]^2. \tag{28}$$

The radiation time $\phi_i(k)$ of kth pulse pair is calculated as

$$\phi_i(k) = \phi_i(0) + kT_I. \tag{29}$$

Considering the fact that the probability that the value is distributed in $(\mu - 3\sigma, \mu + 3\sigma)$ is 99.74 %, the ith LED possible radiation time set $\mathbf{\Phi}_i$ is calculated as

$$\mathbf{\Phi}_i = \left\{ \phi_i(k) - 3\delta : \frac{\alpha\varepsilon}{c} : \phi_i(k) + 3\delta \right\} \tag{30}$$

where α is utilized to adjust the time step to search the target signal more effectively in the time domain. Based on the given $\mathbf{\Phi}_i$, the likelihood ratio γ is calculated as

$$\gamma = \sum_{k=1}^{K} \sum_{i=1}^{4} \left| y_{\mathrm{re},i}(k) - \sqrt{P \times w_{\phi_i}^{j}(k) \times T_{\mathrm{w}}} \times h_i^j \right|. \tag{31}$$

Finally, when γ is found, the optimal estimates of the radiation time $\hat{\phi}_i(k)$ and position $\hat{\mathbf{q}}_j$ of γ are obtained

$$[\hat{\phi}_i(k), \hat{\mathbf{q}}_j] = \max(\gamma). \tag{32}$$

IV. EXPERIMENTAL TESTBED AND RESULT ANALYSIS

An experimental testbed is constructed to verify the effectiveness of the proposed positioning scheme in the typical $5 \times 5 \times 3$ m^3 scenario. Based on the mutually prime principle and the maximum transmission delay, the pulse intervals T_{i} of LED1-LED4 are set as 11, 7, 3, and 5 μs, respectively. The considering LED transmitter tags, reference point, and other simulation parameters are shown in Table I.

Fig. 7 depicts the structure of the semiphysical experimental testbed and the detail of the transceiver front end. Specifically, the proposed OOK-based beacon generation is realized by the field programmable gate arrays (FPGA) board (ZYNQ7000-XC7Z035). First, an oscilloscope with a low sampling rate of 100 MHz is exploited to measure the signal received by PD. Note that the receiver locations of PD involved in the experimental analysis follow a uniform distribution. Then, the measured signal is filtered and the corresponding positioning beacon signal is reconstructed with high precision after filtering. Finally, the measured data are processed with MATLAB. Based on the semiphysical experimental setting, the performance results of positioning are analyzed in the following.

First, the characteristic of the positioning beacon is analyzed. Fig. 8 shows the transmission beacon waveform of each LED

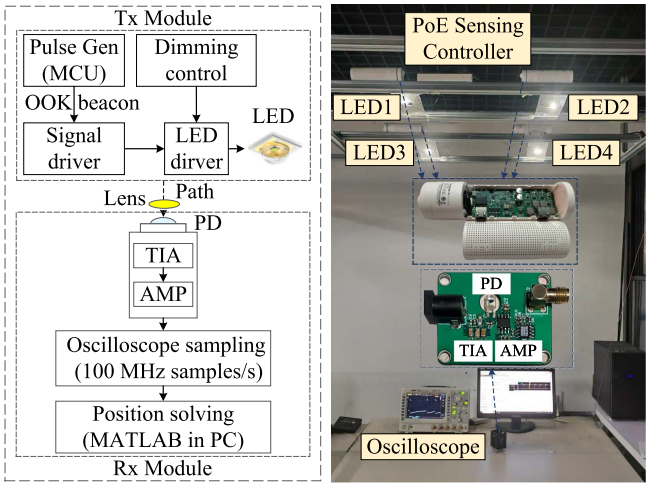

Fig. 7. Structure of the semiphysical experimental testbed.

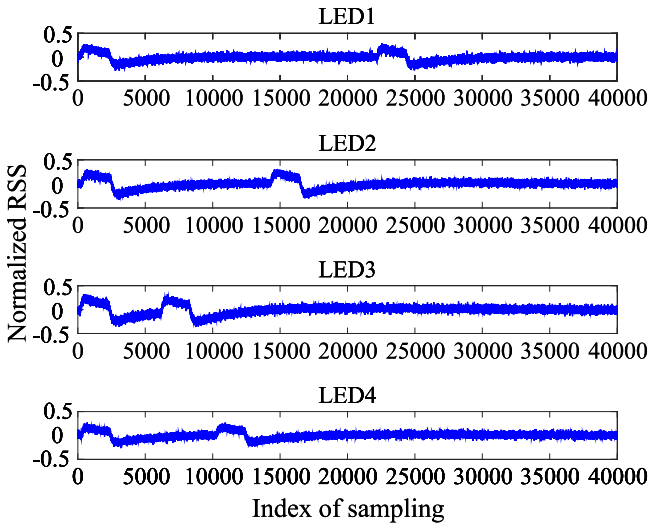

Fig. 8. Transmission beacon waveform of each LED.

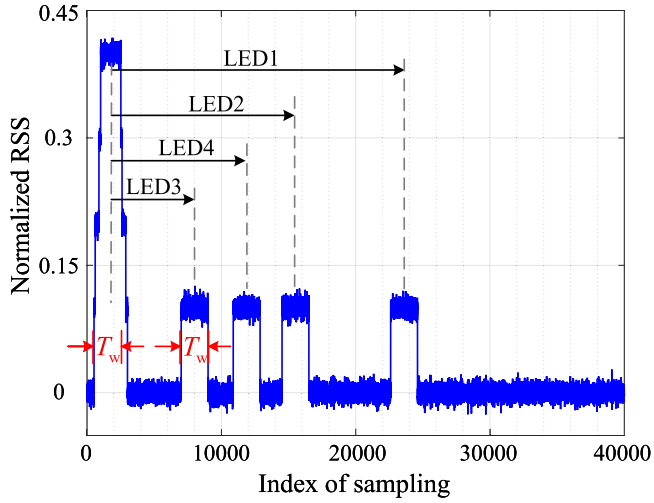

Fig. 9. Received beacon waveform at the center point.

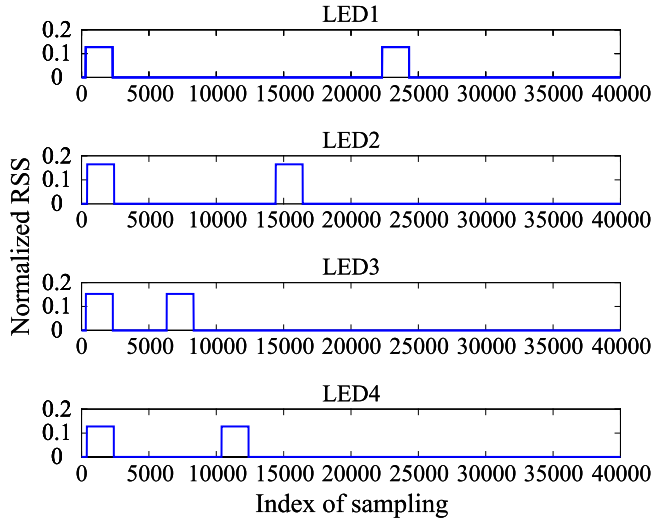

Fig. 10. Beacon waveforms recovered from each LED using the proposed reconstruction method.

to the reference position point. It can be seen from Fig. 8 that the transmission beacon has experienced severe distortion due to the LED driving and photoelectric conversion. Thus, an efficient signal recovery is meaningful. Fig. 9 shows the received waveform at the reference point. It can be seen that the highest pulse consists of the first pulse of the four LED pulse pairs. In other words, although the propagation time error of different LEDs results in the width of the first received pulse being wider than the other pulses, the first pulse of the four LED pulse pairs arrives at the reference point almost simultaneously. Thus, it is beneficial for the receiver to extract the arrival time of the beacon. Moreover, the high level of each pulse has numerous and nonnegligible glitches. This also reveals that high-precision pulse reconstruction is very urgent in a resource-limited scenario with a low sampling rate. Fig. 10 depicts the beacon waveforms recovered and extracted by using the proposed high-precision pulse reconstruction method. This verifies the effectiveness of the proposed pulse reconstruction method. Thus, the corresponding relationship between the received pulse pair and the transmitted LED, the time of arrival (TOA), and RSS of each pulse pair can be obtained by decoding the pulse pair.

Second, the performance comparison is conducted to further verify the effectiveness of the proposed positioning scheme. Specifically, the positioning performance of 2000 uniformly distributed locations was utilized for subsequent statistical evaluation. Fig. 11 depicts the cumulative distribution function (CDF) related to positioning error with different sampling rates. Note that the transmit signal-to-noise ratio (SNR) is set as 30 dB and the green curve is reconstructed from 100 MHz to 2 GHz. It can be observed that the CDF achieved by positioning with pulse reconstruction significantly outperforms that obtained by positioning without pulse reconstruction. Moreover, the positioning performance achieved by the reconstruction-based 2 GHz pulse is close to that obtained by the original 2 GHz sampling pulse. The result confirms the effectiveness of the high-precision pulse reconstruction method.

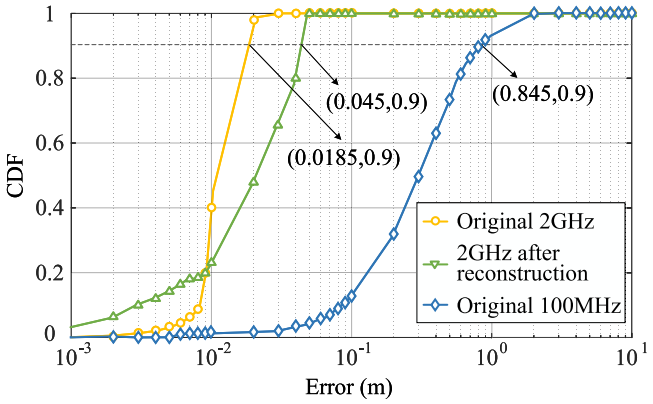

Fig. 11. CDF related to the location estimation error with and without high-precision pulse reconstruction.

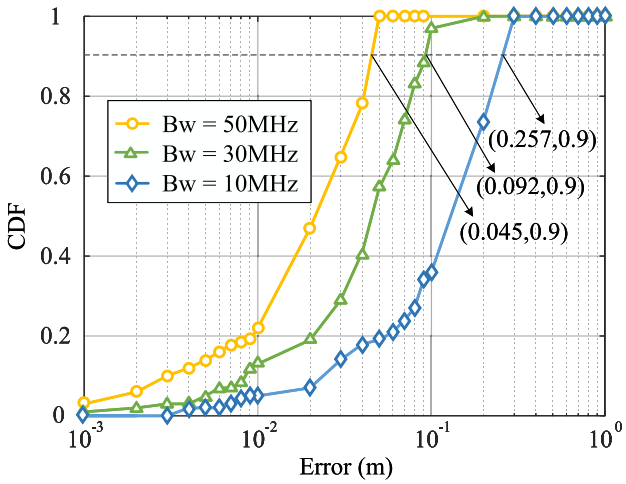

Fig. 12. CDF versus the bandwidth.

Third, the positioning performance under different conditions is evaluated. Specifically, Fig. 12 shows the CDF of positioning error achieved by the proposed positioning scheme versus the bandwidth. Note that the transmit SNR is set as 30 dB and the reconstructed sampling rate is 2 GHz. It can be observed that positioning performance in 90% positioning error corresponding to 50, 30, and 10 MHz bandwidth of LED is 4.5, 9.2, and 25.7 cm, respectively. In other words, the positioning performance decreases with the decreasing bandwidth. This is attributed to the fact that the LED with higher bandwidth can provide a flatter response and, thus, the corresponding beacon waveform is closer to the rectangle waveform. It is worth emphasizing that the positioning accuracy remains within 30 cm, even if the bandwidth of LED is generally less than 10 MHz. Fig. 13 illustrates the CDF of positioning error achieved by the proposed positioning scheme versus the transmit SNR. Note that the bandwidth of LED is set as 50 MHz and the reconstructed sampling rate is 2 GHz. Moreover, the transmitter power is fixed at a specific value in the semiphysical experimental measurement. Subsequently, different levels of additive white Gaussian noise are added to the actual signals measured by the oscilloscope during MATLAB processing to simulate the desired SNR. It can be seen that the positioning performance increases with the

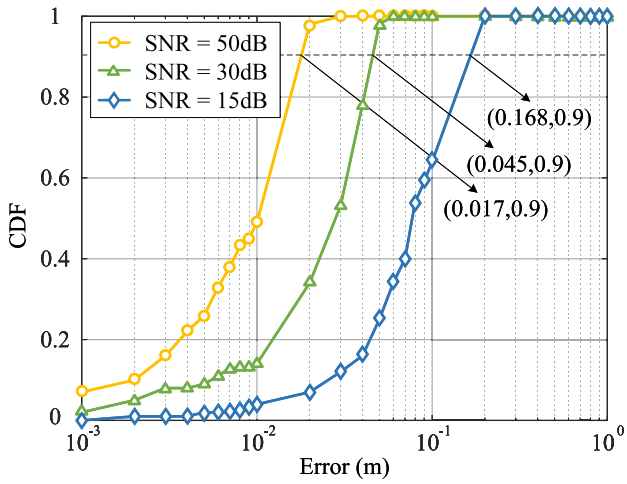

Fig. 13. CDF versus the transmit SNR.

increasing transmit SNR. Specifically, positioning performance corresponding to 50, 30, and 15 dB transmit SNR is 1.7, 4.5, and 16.8 cm, respectively. The experimental results further demonstrate that the proposed positioning scheme achieves high positioning performance even under low bandwidth conditions.

Finally, the positioning performance achieved by the proposed positioning method is compared with the existing benchmark positioning methods, namely DPDOA, CA-RSS, TDOA, and RSS. Among them, DPDOA utilizes the propagation time and phase differences of optical signals at different locations to determine the position of the receiver [26]. CA-RSS analyzes visual information captured by cameras to determine the relationship between LED and receivers and then locates the receiver by the received optical signal strength [27]. TDOA involves measuring the time differences in light signal reception among different receivers and using this time difference information along with known transmitter positions and localization algorithms, the position of the receiver can be determined [14]. In addition, RSS involves measuring the received signal strength and employing a signal strength decay model to convert the signal strength into distance estimates and then uses the multiple-point positioning algorithms to calculate the position of the receiver based on these estimates [28]. In order to focus on the performance comparison, the positioning performance of the benchmark methods are obtained through simulation in the same scenario setting. Fig. 14 depicts the CDF of positioning error achieved by different methods in the case of a 30 dB transmit SNR. It can be observed that the positioning accuracy of the five positioning methods corresponding to 90% positioning error is 0.8, 5, 7.5, 9.2, and 21 cm, respectively. Thus, it can be demonstrated that the proposed positioning method exhibits significantly better positioning performance, emphasizing the effective utilization of the amplitude and timing characteristics of pulse pairs, ultimately optimizing the localization performance.

V. Conclusion

In this article, a novel positioning scheme with beacon design and high-precision pulse reconstruction was proposed in the

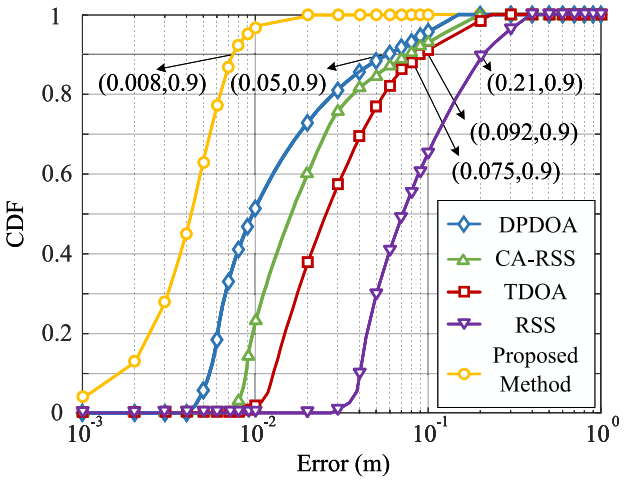

Fig. 14. CDF based on different methods.

PoE-enabled VLP networks to unlock stringent time synchronization and the limitations result from the low modulation bandwidth and the low sampling rate of the transceiver. First, SyncE and PTP were introduced to achieve synchronization transmission. Meanwhile, the modulation-friendly OOK-based pulse pairs was designed to construct the positioning beacon and to address the transceivers' synchronization. Then, by considering the LED equivalent circuit model and pulse response, the high-precision pulse reconstruction was proposed to enhance the signal quality. Moreover, a MAP-based position calculation method is introduced to estimate the location information from the reconstructed received signals. Furthermore, the experimental semiphysical testbed was constructed to verify the effectiveness and feasibility of the proposed positioning scheme. The experimental results demonstrate that the performance achieved by the proposed positioning schemes is better than differential phase difference of arrival, time difference of arrive, received signal strength (RSS), and camera-assisted RSS. Specifically, 90% positioning error achieved by the proposed scheme remains during 1.7 cm under 2 GHz reconstructed sampling rate and 50 MHz bandwidth. In additional, the positioning accuracy keeps 25.7 cm even with just 10 MHz bandwidth.

REFERENCES

[1] X. Huang et al., "A novel experimental visible light positioning system with low bandwidth requirement and high precision pulse reconstruction," in *Proc. IEEE 13th Int. Conf. Indoor Positioning Indoor Navigation*, Nuremberg, Germany, 2023, pp. 1–6.

[2] Z. Wei et al., "Integrated sensing and communication signals toward 5G-A and 6G: A survey," *IEEE Internet. Things J.*, vol. 10, no. 13, pp. 11068–11092, Jul. 2023.

[3] H. Zhou, M. Zhang, and X. Ren, "Design and implementation of wireless optical access system for VLC-IoT networks," *J. Lightw. Technol.*, vol. 41, no. 8, pp. 2369–2380, Apr. 2023.

[4] M. Esteki, S. A. Khajehoddin, A. Safaee, and Y. Li, "LED systems applications and LED driver topologies: A review," *IEEE Access.*, vol. 11, pp. 38324–38358, 2023.

[5] K. Zhang, Z. Zhang, and B. Zhu, "Beacon LED coordinates estimator for easy deployment of visible light positioning systems," *IEEE Trans. Wireless Commun.*, vol. 21, no. 12, pp. 10208–10223, Dec. 2022.

[6] M. F. Keskin, A. D. Sezer, and S. Gezici, "Localization via visible light systems," *Proc. IEEE*, vol. 106, no. 6, pp. 1063–1088, Jun. 2018.

[7] O. Narmanlioglu and M Uysal, "Multi-user massive MIMO visible light communications with limited pilot transmission," *IEEE Trans. Wireless Commun.*, vol. 21, no. 6, pp. 4197–4211, Jun. 2022.

[8] Z. Xiao, "An efficient power over ethernet (PoE) interface with current-balancing and hot-swapping control," *IEEE Trans. Ind. Electron.*, vol. 65, no. 3, pp. 2496–2506, Mar. 2018.

[9] Z. Li, A. Yang, H. Lv, L. Feng, and W. Song, "Fusion of visible light indoor positioning and inertial navigation based on particle filte," *IEEE Photon. J.*, vol. 9, no. 5, pp. 1–13, Oct. 2017.

[10] Y. Hou, S. Xiao, H. Zheng, and W. Hu, "Multiple access scheme based on block encoding time division multiplexing in an indoor positioning system using visible light," *IEEE/OSA J. Opt. Commun. Netw.*, vol. 7, no. 5, pp. 489–495, May 2015.

[11] G. B. Prince and T. D. C. Little, "A. two phase hybrid RSS/AoA algorithm for indoor device localization using visible light," in *Proc. IEEE Glob. Commun. Conf.*, Anaheim, CA, USA, 2012, pp. 3347–3352.

[12] J. Herrnsdorf, M. J. Strain, E. Gu, R. K. Henderson, and M. D. Dawson, "Positioning and space-division multiple access enabled by structured illumination with light-emitting diodes," *J. Lightw. Technol.*, vol. 35, no. 12, pp. 2339–2345, Jun. 2017.

[13] T. Do, J. Hwang, and M. Yoo, "TDoA based indoor visible light positioning systems," in *Proc. 5th Int. Conf. Ubiquitous Future Netw.*, Da Nang, Vietnam, 2013, pp. 456–458.

[14] P. Du, S. Zhang, C. Chen, A. Alphones, and W.-D. Zhong, "Demonstration of a low-complexity indoor visible light positioning system using an enhanced TDOA scheme," *IEEE Photon. J.*, vol. 10, no. 4, pp. 1–10, Aug. 2018.

[15] B. Soner and S. C. Ergen, "Vehicular visible light positioning with a single receiver," in *Proc. IEEE Int. Symp. Person Indoor Mobile Radio Commun.*, Istanbul, Turkey, 2019, pp. 1–6.

[16] J. -P. M. G. Linnartz, X. Deng, A. Alexeev, and S. Mardanikorani, "Wireless communication over an LED channel," *IEEE Commun. Mag.*, vol. 58, no. 12, pp. 77–82, Dec. 2020.

[17] X. Chen et al., "A hybrid active-passive single-order equalizer for visible light communication systems," *IEEE Photonics. Technol. Lett.*, vol. 35, no. 24, pp. 1395–1398, Dec. 2023.

[18] X. Liu, Y. Wang, F. Zhou, S. Ma, R. Q. Hu, and D. W. K. Ng, "Beamforming design for secure MISO visible light communication networks with SLIPT," *IEEE Trans. Commun.*, vol. 68, no. 12, pp. 7795–7809, Dec. 2020.

[19] W. Hennig, V. Thomas, S. Hoover, and O. Delaune, "Network time synchronization of the readout electronics for a new radioactive gas detection system," *IEEE Trans. Nucl. Sci.*, vol. 66, no. 7, pp. 1182–1189, Jul. 2019.

[20] A. Garg, A. Yadav, A. Sikora, and A. S. Sairam, "Wireless precision time protocol," *IEEE Commun. Lett.*, vol. 22, no. 4, pp. 812–815, Apr. 2018.

[21] D. A. Popescu and A. W. Moore, "Measuring network conditions in data centers using the precision time protocol," *IEEE Trans. Netw. Serv. Manage.*, vol. 18, no. 3, pp. 3753–3770, Sep. 2021.

[22] J. Aweya, "Implementing synchronous ethernet in telecommunication systems," *IEEE Commun. Surv. Tutor.*, vol. 16, no. 2, pp. 1080–1113, Second Quarter 2014.

[23] V. M. De Albuquerque, G. M. Soares, J. M. Alonso, and P. S. Almeida, "A simple resonant switched-capacitor LED driver employed as a fast pulse-based transmitter for VLC applications," *IEEE J. Emerg. Sel. Topics Power Electron.*, vol. 9, no. 1, pp. 111–122, Feb. 2021.

[24] D. Shi et al., "Physics-based modeling of GaN MQW LED for visible light communication systems," *IEEE Trans. Electron. Devices*, early access, Sep. 2023, doi: 10.1109/TED.2023.3312632.

[25] T. Liu, T. Jiang, C. Chung, and Y. Chu, "A maximum logarithmic maximum a posteriori probability based soft-input soft-output detector for the coded spatial modulation systems," *IEEE Trans. Circuits Syst. I, Reg. Papers*, vol. 69, no. 9, pp. 3816–3828, Sep. 2022.

[26] S. Zhang, W. Zhong, P. Du, and C. Chen, "Experimental demonstration of indoor sub-decimeter accuracy VLP system using differential PDOA," *IEEE Photon. Technol. Lett.*, vol. 30, no. 19, pp. 1703–1706, Oct. 2018.

[27] L. Bai, Y. Yang, C. Guo, C. Feng, and X. Xu, "Camera assisted received signal strength ratio algorithm for indoor visible light positioning," *IEEE Commun. Lett.*, vol. 23, no. 11, pp. 2022–2025, Nov. 2019.

[28] T. Sato, S. Shimada, H. Murakami, H. Watanabe, H. Hashizume, and M. Sugimoto, "ALiSA: A visible-light positioning system using the ambient light sensor assembly in a smartphone," *IEEE Sensors J.*, vol. 22, no. 6, pp. 4989–5000, Mar. 2022.

Zhenghai Wang (Member, IEEE) received the B.Sc. and Ph.D. degrees in information and communication system from the Electronic Information School, Wuhan University, Wuhan, China, in 2006 and 2011, respectively.

From 2011 to 2018, he was with the CETC Key Laboratory of Avionic Information System Technology, Chengdu, China, as a Senior Engineer in wideband radar and communication signal processing. He is currently a Professor with the Information Engineering School, Nanchang University, Nanchang, China. His research interests include integrated sensing and communication by radio and visible light in extreme environments.

Xuan Huang (Graduate Student Member, IEEE) received the B.Sc. degree in electronic information engineering from Hubei Polytechnic University, Huangshi, China, in 2022. She is currently working toward the M.Sc. degree in new generation of electronic information technology with the School of Information Engineering, Nanchang University, Nanchang, China.

Her major is the new generation of electronic information technology. Her research interests focus on visible light positioning.

Xuanbang Chen (Graduate Student Member, IEEE) received the B.Sc. degree in information and communication engineering from Nanchang University, Nanchang, China, in 2019. He is currently working toward the Ph.D. degree in information and communication engineering with the School of Information Engineering, Nanchang University, Nanchang, China. He is also a joint supervised Ph.D. candidate student at Sorbonne University, Paris, France.

His research interests include LED performance characterization and hardware fingerprint for visible light-based integrated sensing and communication.

Mengzhen Xu (Student Member, IEEE) received the M.Sc. degree in communication engineering from Nanchang University, Nanchang, China, in 2023.

Her main interests include visible light positioning and visible light in extreme environments.

Xiaodong Liu (Member, IEEE) received the Ph.D. degree in information and communication system from Wuhan University, Wuhan, China, in 2021.

He is currently an Associate Professor with the School of Information Engineering, Nanchang University. He is also a Research Fellow with Institut superieur d'lectronique de Paris, Paris, France. His research interests focus on visible light communication and positioning, non-orthogonal multiple access, channel measurement and modeling, physical layer security, and resource allocation. He has been involved in an international project Horizon H2020 6G BRAINS.

Yuhao Wang (Senior Member, IEEE) received the Ph.D. degree in space physics from Wuhan University, Wuhan, China, in 2006.

He was a Visiting Professor with the Department of Electrical Communication Engineering, University of Calgary, Calgary, AB, Canada, in 2008, and also with China National Mobile Communication Research Laboratory, Southeast University, Nanjing, China, from 2010 to 2011. He is currently a Professor with the multifunctional Optical/RF Sensor and AI (FORSEAI) Laboratory, School of Information Engineering, Nanchang University, Nanchang, China. He is the Deputy Secretary of Shangrao Normal University. Since 2016, he is an IET Fellow. His current research interests include integration of illumination, communication and sensing system, channel measurement and modeling, nonlinear signal processing, smart sensor, and machine learning.

Xun Zhang (Senior Member, IEEE) received the Ph.D. degree in the instrumentation and microelectronics (IM) science from the University of Nancy, Nancy, France, in 2009.

From 2009 to 2011, he completed a Post-Doc in the SCEE Laboratory in CentralSupelec, France, under the supervision of Pr. Jacques Palicot. He joined the LISITE laboratory in ISEP in 2011 as an Associate Professor. He is currently a Professor in ISEP, Paris, France. His current research interests are PHY layer optimization for 5G cellular networks and VLC systems, and VLC-based indoor high accuracy positioning algorithm and tracking algorithm. He has been involved in serval international projects (Horizon H2020 6 G BRAINS, Horizon H2020 IoRL, EGIDE Franco-Chine, CAIYUANPEI, XUGUANGQI, and Orange foundation RoBo).